

Solving Hamilton-Jacobi equations by minimizing residuals of monotone discretizations

O. Bokanowski^{*1}, C. Esteve-Yaguë^{†2}, and R. Tsai^{‡3}

¹Laboratoire Jacques-Louis Lions, Université Paris Cité, France

²Departamento de Matemáticas, Universidad de Alicante, Spain

³Department of Mathematics and Oden Institute, The University of Texas at Austin, USA

January 30, 2026

Abstract

We derive sufficient conditions under which residual minimization yields well-posed discrete solutions for nonlinear equations defined by monotone finite-difference discretizations. Our analysis is motivated by the challenge of solving fully nonlinear Hamilton-Jacobi (HJ) equations in high dimensions by means of a Neural Network, which is trained by minimizing residuals arising from monotone discretizations of the Hamiltonian. While classical theory ensures that consistency and monotonicity imply convergence to the viscosity solution, treating these discrete systems as optimization problems introduces new analytical hurdles: solvability and the uniqueness of local minima do not follow from monotonicity alone.

By establishing the well-posedness of these optimization-based solvers, our framework enables the adaptation of Level Set Methods to high-dimensional settings, unlocking new capabilities in applications such as high-dimensional segmentation and interface tracking. Finally, we observe that these arguments extend almost directly to degenerate elliptic or parabolic PDEs on graphs equipped with monotone graph Laplacians.

Keywords: Hamilton-Jacobi equations; viscosity solutions; physics-informed neural networks; finite-difference residuals; optimal control theory.

AMS Subject Classification (2020): 49L25, 35A15, 68T07, 49K20, 65N06

^{*}olivier.bokanowski@u-paris.fr

[†]c.esteve@ua.es

[‡]ytsai@math.utexas.edu

1 Introduction

Hamilton–Jacobi (HJ) equations are ubiquitous in mathematical physics and control theory, governing systems ranging from level-set dynamics to high-dimensional mean-field games. We consider the fully nonlinear equation:

$$H(x, u, \nabla u(x)) = 0, \quad x \in \Omega \subset \mathbb{R}^d, \quad (1)$$

with boundary data $u|_{\Gamma} = g$ and the time dependent version

$$u_t + F(x, u, \nabla u(x)) = 0, \quad x \in \Omega \subset \mathbb{R}^d, t > 0, \quad (2)$$

with initial condition $u(x, 0) = u_0(x)$ in Ω and boundary data $u|_{\Gamma} = g$.

Solving these problems poses multiple challenges. First, the solution u is generally not C^1 , requiring the non-classical notion of *viscosity solutions* to handle inherent non-smoothness. While the Barles–Souganidis theorem [2] theoretically guarantees that monotone, consistent, and stable schemes converge to this weak solution, implementing such schemes in high-dimensional domains remains historically prohibitive due to exponential complexity for discretizing the domain.

Classical numerical methods for solving Hamilton–Jacobi equations, such as the Fast Marching Methods [17][14, 15] and Fast Sweeping Methods [18, 16, 9], rely on discretizing the PDE, typically on a grid. While effective in low dimensions, this approach is fundamentally infeasible for high-dimensional problems because the size of the discretized system grows exponentially with dimension.

In [5],[4],[3], grid-free algorithms are developed for Hamilton–Jacobi equations; the algorithms leverage classical representation formulas, such as Hopf–Lax and Lax–Oleinik, and fast optimization methods. Instead of necessarily solving a consistent discretization of the PDE everywhere or wrestling with the convergence issues of shooting methods, his algorithms compute the solution value at any given query point, formally with a complexity that is not exponentially growing. Recently, [10] introduces a neural implicit solution formula that generalizes the classical Hopf and Lax formulas, utilizing deep learning to efficiently solve high-dimensional, state-dependent, and nonconvex Hamilton–Jacobi equations.

The computational infrastructure developed for deep learning has provided new tools to mitigate some of the computational challenges. By exploiting function approximators (deep neural networks) and optimization landscapes native to modern AI workflows, we introduce a numerical methodology that respects the viscosity framework while scaling more effectively to high dimensions.

Specifically, we propose to construct numerical approximations by minimizing residual functionals defined via consistent and monotone numerical Hamiltonians. By formulating the loss function in terms of these discretized operators rather than the continuous PDE directly, we firmly anchor our learning procedure in the theoretical convergence framework established by Barles and Souganidis [2].

The computational framework studied here was introduced in [6], where the authors showed that, for Lax–Friedrichs discretizations with sufficient numerical viscosity, the gradient descent iterations form a well-posed problem that converges to a unique global minimizer. Notably, [6] presented numerical experiments carried out on a single laptop, solving

Eikonal equations in dimensions as high as 10 and 20. These results indicate that the method can scale to high-dimensional settings that are typically beyond the reach of classical grid-based schemes, offering a path to mitigate the computational bottlenecks inherent to high-dimensional PDEs. The present work generalizes that analysis to a broader class of monotone discretizations, including Upwind and Godunov schemes. Furthermore, we investigate how the optimization landscape depends on the discretization parameter, providing a theoretical basis for the observation that training with larger grid spacing yields faster convergence and improved data efficiency. These insights motivate the multi-level 'warm-start' strategies that are essential for applying the method to higher-dimensional problems.

Residual minimization based on discrete monotone schemes. In recent years, optimization and machine-learning techniques have inspired the development of approaches based on minimizing the residuals of a partial differential equation (PDE). A common approach, popularized by Physics-Informed Neural Networks (PINNs) [12] and Deep Galerkin Methods (DGMs), minimizes the squared L^2 norm of the *continuous PDE residual* $H(x, \nabla u(x))$ evaluated on collocation points. However, for nonlinear and nonconvex equations such as (1), minimizing the continuous residual does not guarantee convergence to the viscosity solution. A crucial reason is that multiple weak solutions of PDE may produce identical zero-residual values. This is particularly the case for Hamilton-Jacobi equations.

To address the issue of non-uniqueness of weak solutions, we adopt a residual-minimization framework based on a consistent and convergent *numerical scheme*, rather than on the continuous PDE. This approach relies on the fundamental convergence result of Barles and Souganidis [2], which guarantees that the solution of a numerical scheme converges to the unique viscosity solution provided the scheme is stable, monotone, and consistent.

In this paper, we consider numerical schemes defined on a set of points $\{x_j\} \subset \overline{\Omega}$:

$$\mathcal{H}\left(x_j, u_j, \left\{\frac{u_j - u_k}{\Delta x_{jk}}\right\}_{k \in \mathcal{V}_j}\right) = 0, \quad x_j \in \Omega \setminus \Gamma, \quad \text{and} \quad u_j = g(x_j), \quad x_j \in \Gamma \quad (3)$$

where \mathcal{V}_j is the index set associated to a finite set $\{x_{jk}\}_{k \in \mathcal{V}_j} \subset \overline{\Omega}$ of neighboring points of x_j ; and $\left\{\frac{u_j - u_k}{\Delta x_{jk}}\right\}_{k \in \mathcal{V}_j}$ is the set of finite differences used to approximate the directional derivatives of u at x_j in the directions $v_{jk} = \frac{x_j - x_k}{\Delta x_{jk}}$. For the boundary value problem (1), we shall consider loss functionals of the form

$$L(u) := \sum_{j \in \mathcal{J}} \left(\mathcal{H}\left(x_j, u_j, \left\{\frac{u_j - u_k}{\Delta x_{jk}}\right\}_{k \in \mathcal{V}_j}\right) \right)^2 + \mu_b \sum_{j \in \mathcal{B}} (u_j - g(x_j))^2, \quad (4)$$

where \mathcal{J} and \mathcal{B} are the index sets for the points x_j belonging to the interior of the domain and to the boundary respectively.

Our objective is to construct, efficiently, neural networks $u(x; \theta)$ whose restriction to the points $(x_j)_{j \in \mathcal{J} \cup \mathcal{B}}$ is the solution of the numerical scheme (3), satisfying the given boundary data. For that, we minimize a loss functional $L(u)$ of the form (4) over a class of neural networks $\mathcal{M} = \{u(\cdot; \theta) : \theta \in \mathbb{R}^m\}$, which is a family of continuous functions parameterized

by a set of parameters $\theta \in \mathbb{R}^m$. A natural route is to minimize $L(u(\cdot; \theta))$ over the parameters θ , by a variant of the gradient descent method, based on the equation

$$\frac{d}{dt}\theta = -\nabla_\theta L(u(\cdot, \theta)) = -\left\langle \frac{\delta L}{\delta u}, \nabla_\theta u \right\rangle_{\ell^2},$$

where $\delta L/\delta u$ is the gradient of L with respect to the vector $u = (u_j)_{j \in \mathcal{J} \cup \mathcal{B}}$.

We see that the flow converges to two types of stationary points: ones which correspond to the critical point of L , and the others at which the $\delta L/\delta u$ is orthogonal to the tangent space of $\mathcal{M} = \{u(\cdot, \theta) : \theta \in \mathbb{R}^m\}$.

The gradient flow in the parameter space induces a flow on \mathcal{M} :

$$\frac{\partial}{\partial t}u(x, \theta(t)) = -\left\langle \frac{\delta L}{\delta u}, \nabla_\theta u \right\rangle_{\ell^2} \nabla_\theta u$$

this can be interpreted as applying semi-positive definite preconditioners $\nabla_\theta u \otimes \nabla_\theta u$ to the gradient flow

$$\frac{\partial}{\partial t}u(x, t) = -\frac{\delta L}{\delta u},$$

resulting in possible spectral bias in convergence rates. In any case, it is essential to analyze whether any critical point of $L(u)$ yield a numerical solution to the discrete Hamilton-Jacobi equation with prescribed boundary data.

Observations. A central discovery of this work is that, for time-dependent HJ equations, the uniqueness of the global minimizer of the residual functional associated with an *implicit* (backward-Euler) monotone scheme essentially have no restriction on the time step Δt . In contrast, explicit schemes, which require a CFL condition for stability in time-marching, do not require any such condition for solvability of the residual minimization problem.

From a computational standpoint, both explicit and implicit residual formulations lead to comparable convergence behavior in iterative solvers. Therefore, implicit formulations do not incur additional computational difficulties in residual-minimization approaches to Hamilton-Jacobi problems. Moreover, since our analysis depends only on monotonicity and Lipschitz continuity of \mathcal{H} , the same algebraic framework extends almost directly to degenerate elliptic and parabolic PDEs, including those posed on graphs where ∇_G corresponds to a monotone graph Laplacian. This perspective unifies classical finite-difference analysis with emerging optimization-based formulations for nonlinear PDEs.

Organization. The paper is structured to establish a theoretical foundation for solving Hamilton-Jacobi (HJ) equations through optimization-based residual minimization. Section 2 details the setup of monotone numerical schemes and their associated residual functionals, defining the problem on geometrical graphs and establishing the well-posedness of the optimization approach. This section includes proofs for the existence and uniqueness of critical points (Theorem 1), stability results (Theorem 2), and practical examples of monotone Hamiltonians such as Lax-Friedrichs and Upwind schemes. Section 3 extends this framework to time-dependent problems, highlighting the structural differences between spatial and temporal dimensions and the implications for numerical stability conditions. Section 4

presents the algorithmic implementation of the proposed residual minimization framework, specifically detailing the integration with deep neural networks. Finally, Section 5 provides a few computational examples.

2 Monotone schemes and their residual functionals

We define a **geometrical graph** $G = (V, E, W)$ embedded in a domain $\bar{\Omega} \subset \mathbb{R}^d$. The vertex set V is identified with a set of points $X = \{x_j\}_{j \in V} \subset \mathbb{R}^d$. We partition the index set V into two disjoint finite sets as follows:

$$V = \mathcal{J} \cup \mathcal{B}, \quad \text{with} \quad \mathcal{J} \cap \mathcal{B} = \emptyset. \quad (5)$$

Here, \mathcal{J} represents the indices of *interior nodes*, such that $\{x_j : j \in \mathcal{J}\} \subset \Omega$, and \mathcal{B} represents the indices of *boundary nodes*, such that $\{x_j : j \in \mathcal{B}\} \subset \partial\Omega$.

The set of edges $E \subseteq V \times V$ represents the connectivity between points. An edge $(i, j) \in E$ exists if the node j is in the local neighborhood of i (e.g., within a connectivity radius δ or among the k -nearest neighbors). We denote the set of neighbors of node i as $\mathcal{V}_i = \{j \in V : (i, j) \in E\}$.

Between two connected nodes, we define the edge weights by $1/\Delta x_{ij}$. Typically, for the problems in Euclidean domains, $\Delta x_{ij} = \|x_j - x_i\|_2$ is the Euclidean distance between the two nodes. We further assume that $C_1\Delta x \leq \Delta x_{ij} \leq C_2\Delta x$ for some constants $C_1, C_2 > 0$ and for all $i \in \mathcal{J} \cup \mathcal{B}$ and $j \in \mathcal{V}_i$.

We consider the following problem with unknowns u_j for $j \in \mathcal{J}$

$$\mathcal{H}(x_j, u_j, \nabla_G u_j) = 0, \quad j \in \mathcal{J}, \quad (6)$$

and given boundary values

$$u_j = g_j, \quad j \in \mathcal{B}. \quad (7)$$

$\mathcal{H}(x_j, \cdot, \cdot) : \mathbb{R} \times \mathbb{R}^{|\mathcal{V}_j|} \rightarrow \mathbb{R}$ is a “numerical Hamiltonian” depending on a set of finite differences

$$\nabla_G u_j := \left\{ \frac{u_j - u_k}{\Delta x_{kj}} \right\}_{k \in \mathcal{V}_j}, \quad \Delta x_{kj} > 0,$$

involving “neighboring values” u_k , $k \in \mathcal{V}_j$. In particular, $x_j \notin \mathcal{V}_j$. We furthermore assume, for simplicity of presentation, that $|\mathcal{V}_j| = K$ is constant, $\forall j \in \mathcal{J}$ (for a given $K \in \mathbb{N}^*$), and

$$\forall k \neq j, \quad \Delta_{k,j} = \Delta_{j,k} \text{ and } k \in \mathcal{V}_j \quad \Leftrightarrow \quad j \in \mathcal{V}_k.$$

2.1 The residual function and well-posedness

Let $M = |\mathcal{J}|$ and $N = |\mathcal{B}|$ be the number of interior and boundary points respectively. We represent any function on $\mathcal{J} \cup \mathcal{B}$ by a vector $u := \{u_j : j \in \mathcal{J} \cup \mathcal{B}\} \in \mathbb{R}^{M+N}$.

For given $q > 1$ and $\mu_b > 0$, we define the residual function $\mathcal{R} : \mathbb{R}^{M+N} \rightarrow \mathbb{R}^{M+N}$ as

$$\mathcal{R}(u)_j := \begin{cases} \frac{1}{M^{1/q}} \mathcal{H}(x_j, u_j, \nabla_G u_j), & \text{if } j \in \mathcal{J}, \\ \left(\frac{\mu_b}{N}\right)^{1/q} (u_j - g_j), & \text{if } j \in \mathcal{B}. \end{cases} \quad (8)$$

Note that $u \in \mathbb{R}^{M+N}$ is a solution of (6)-(7) if and only if $\mathcal{R}(u) = 0$.

Our main contribution, summarized in Theorem 1, establishes that the functional

$$L(u) := \frac{1}{q} \|\mathcal{R}(u)\|_q^q = \frac{1}{qM} \sum_{j \in \mathcal{J}} [\mathcal{H}(x_j, u_j, \nabla_G u_j)]^q + \frac{\mu_b}{qN} \sum_{j \in \mathcal{B}} (u_j - g_j)^q, \quad (9)$$

has a unique critical point u^* which coincides with the unique solution to (6)-(7), provided that the numerical Hamiltonian satisfies hypotheses **(H1)-(H3)**:

- (H1)** for all x_j , $(u, p) \mapsto \mathcal{H}(x_j, u, p)$ is Lipschitz continuous;
- (H2)** for all (x_j, u) , the map $p \mapsto \mathcal{H}(x_j, u, p)$ is non-decreasing in all the variables of p ;
- (H3)** there exists a constant $\lambda > 0$ such that

$$\forall j \in \mathcal{J}, \forall u \geq v \in \mathbb{R}, \forall p \in \mathcal{R}^{|\mathcal{V}_j|} \quad \mathcal{H}(x_j, u, p) - \mathcal{H}(x_j, v, p) \geq \lambda(u - v).$$

(note that because of (H1), then (H3) is equivalent to have $\frac{\partial \mathcal{H}}{\partial u}(x_j, u, p) \geq \lambda$ for all j , all p and a.e. $u \in \mathbb{R}$).

The first step to prove that any critical point of $L(u)$ is the unique solution of $\mathcal{R}(u) = 0$ is to prove that for any $u \in \mathbb{R}^{M+N}$ where \mathcal{R} is differentiable, the Jacobian is an invertible matrix with inverse bounded independently of u .

Lemma 1. *Assume that the Hamiltonian function \mathcal{H} satisfies (H1)-(H3). For some $\mu_b > 0$ and $p > 1$, consider the function \mathcal{R} defined in (8). Then, for any $u \in \mathbb{R}^{M+N}$ where \mathcal{R} is differentiable, the Jacobian matrix $D\mathcal{R}(u)$ is μ -diagonally dominant with*

$$\mu = \min \left(\frac{\lambda}{M^{1/q}}, \left(\frac{\mu_b}{N} \right)^{1/q} \right). \quad (10)$$

Therefore, $D\mathcal{R}(u)$ is invertible with $\|(D\mathcal{R}(u))^{-1}\| \leq \frac{1}{\mu}$.

Proof. We recall that, for $\mu > 0$, a square matrix $A \in \mathbb{R}^{(M+N) \times (M+N)}$ is said to be μ -diagonally dominant if $|A_{jj}| \geq \mu + \sum_{k \neq j} |A_{jk}|$ for $1 \leq j \leq M+N$. By Gershgorin theorem, if A is μ -diagonally dominant, all the eigenvalues of A have complex modulus bigger or equal than μ , and therefore, A is invertible with $\|A^{-1}\| \leq \frac{1}{\mu}$.

Recall that $\nabla_G u_j := (\frac{u_j - u_k}{\Delta x_{kj}})_{k \in \mathcal{V}_j}$. For any $j \in \mathcal{J}$ and $k \in \mathcal{V}_j$, let us denote by p_k the variable of $\mathcal{H}(x_j, u_j, \hat{D}u_j)$ receiving the value $p_k = \frac{u_j - u_k}{\Delta x_{kj}}$. Then, for any $j \in \mathcal{J}$ we have

$$\frac{\partial \mathcal{R}(u)_j}{\partial u_j} = \frac{1}{M^{1/q}} \frac{\partial \mathcal{H}}{\partial u}(x_j, u_j, \nabla_G u_j) + \frac{1}{M^{1/q}} \sum_{k \in \mathcal{V}_j} \frac{1}{\Delta x_{kj}} \frac{\partial \mathcal{H}}{\partial p_k}(x_j, u_j, \nabla_G u_j), \quad (11)$$

and for all $k \in \mathcal{V}_j$, we have

$$\frac{\partial \mathcal{R}(u)_j}{\partial u_k} = -\frac{1}{M^{1/q}} \frac{1}{\Delta x_{kj}} \frac{\partial \mathcal{H}}{\partial p_k}(x_j, u_j, \nabla_G u_j). \quad (12)$$

For $k \notin \mathcal{V}_j \cup \{j\}$, we have $\frac{\partial \mathcal{R}(u)_j}{\partial u_k} = 0$. Because of the monotonicity assumptions **(H2)**-**(H3)**,

$$\begin{aligned} \left| \frac{\partial \mathcal{R}(u)_j}{\partial u_j} \right| &\geq \frac{\lambda}{M^{1/q}} + \frac{1}{M^{1/q}} \sum_{k \in \mathcal{V}_j} \frac{1}{\Delta x_{kj}} \frac{\partial \mathcal{H}}{\partial p_k}(x_j, u_j, \nabla_G u_j) \\ &= \frac{\lambda}{M^{1/q}} + \sum_{k \in \mathcal{V}_j} \left| \frac{1}{M^{1/q}} \frac{1}{\Delta x_{kj}} \frac{\partial \mathcal{H}}{\partial p_k}(x_j, u_j, \nabla_G u_j) \right| \\ &= \frac{\lambda}{M^{1/q}} + \sum_{k \neq j} \left| \frac{\partial \mathcal{R}(u)_j}{\partial u_k} \right|, \quad j \in \mathcal{J}. \end{aligned}$$

Hence, all the rows in the Jacobian with index $j \in \mathcal{J}$ are μ -diagonally dominant with $\mu_1 = \frac{\lambda}{M^{1/q}}$.

For any $j \in \mathcal{B}$, the corresponding row is trivially μ_2 -diagonally dominant with $\mu_2 = (\mu_b/N)^{1/q}$, since

$$\frac{\partial \mathcal{R}(u)_j}{\partial u_j} = \left(\frac{\mu_b}{N} \right)^{1/q}, \quad \text{and} \quad \frac{\partial \mathcal{R}(u)_j}{\partial u_k} = 0 \quad \forall k \neq j. \quad (13)$$

Therefore, $D\mathcal{R}(u)$ is μ -diagonally dominant with $\mu = \min(\mu_1, \mu_2)$, and therefore, $D\mathcal{R}(u)$ is invertible with $\|(D\mathcal{R}(u))^{-1}\| \leq \frac{1}{\mu}$. \square

We are now in position to prove the main result of this section.

Theorem 1 (Well-posedness of residual minimization). *Under assumptions **(H1)**-**(H3)**, the solution of (6)-(7) exists and is unique. Moreover, for any $\mu_b > 0$ and $q > 1$, this solution is the unique critical point of the functional $L(u)$ defined in (9), in the sense that*

$$0 \in \partial L(u) \quad \text{if and only if} \quad \mathcal{R}(u) = 0,$$

where $\partial L(u)$ denotes the generalized differential¹ of $L(u)$.

Proof. We shall first prove that the problem (6)-(7) has a unique solution, and then we will prove that this solution is indeed the unique critical point of $L(u)$.

(1) *Existence and uniqueness of solution for $\mathcal{R}(u) = 0$.* Let us first assume that the Hamiltonian function $\mathcal{H}(x_j, u_j, \nabla_G u_j)$ is a regular C^1 function of all its variables. Then, by Lemma 1, the Jacobian matrix $D\mathcal{R}(u) \in \mathbb{R}^{(M+N) \times (M+N)}$ is invertible for any $u \in \mathbb{R}^{M+N}$ with $\|D\mathcal{R}(u)\|^{-1} \leq 1/\mu$.

By Hadamard's theorem [7], we deduce that the map $u \rightarrow \mathcal{R}(u)$ of \mathbb{R}^{M+N} is a diffeomorphism of \mathbb{R}^{M+N} . In particular, there is a unique u such that $\mathcal{R}(u) = 0$.

In the general case, if \mathcal{H} is only Lipschitz regular, $u \mapsto \mathcal{R}(u)$ is only a.e. differentiable in \mathbb{R}^{M+N} . We consider the generalized differential of $\mathcal{R}(u)$ in the sense of Pourciau [11].

¹The generalized differential of an a.e. differentiable functional $L : \mathbb{R}^{M+N} \rightarrow \mathbb{R}$, denoted by $\partial L(u)$, is defined as the convex hull of all the possible limits of the classical gradient $\nabla L(u_n)$ as $u_n \rightarrow u$.

We observe that for any element $A \in D\mathcal{R}(u)$ (the generalized differential, defined as the convex hull of all possible limits of the a.e. differentiable function $v \rightarrow \mathcal{R}(v)$ as $v \rightarrow u$), A has the same diagonally dominant structure. Here we also make use of the sign properties of the matrices $B = D\mathcal{R}(v)$ when it is differentiable: $B_{jj} \geq 0$ ($\forall j$) and $B_{jk} \leq 0$ ($\forall j \neq k$), so that convex combination of such matrices B keep the same diagonally dominant bound. Therefore any $A \in D\mathcal{R}(u)$ satisfies $\|A^{-1}\|_\infty \leq \frac{1}{\mu}$. By a generalization of Hadamard's theorem by Pourciau [11], this is enough to conclude that \mathcal{R} is a homeomorphism on \mathbb{R}^{M+N} . Consequently, there is a unique u such that $\mathcal{R}(u) = 0$.

(2) *Characterization as the critical point of $L(u)$.* Here we prove that u^* satisfies $0 \in \partial L(u^*)$ if and only if $\mathcal{R}(u^*) = 0$. Let us first assume that $L(u)$ is differentiable at u^* . Then, $0 \in \partial L(u^*)$ is equivalent to $\nabla L(u^*) = 0$. We define the vector of residuals $w := [\mathcal{R}(u^*)]^{q-1} \in \mathbb{R}^{M+N}$, whose components are given by

$$w_j = \begin{cases} \frac{1}{M^{\frac{q-1}{q}}} [\mathcal{H}(x_j, u_j^*, \nabla_G u_j^*)]^{q-1} & \text{if } j \in \mathcal{J} \\ \left(\frac{\mu_b}{N}\right)^{\frac{q-1}{q}} (u_j^* - g_j)^{q-1} & \text{if } j \in \mathcal{B}. \end{cases}$$

By the definition of $L(u)$ in (9), we can write the gradient as

$$\nabla L(u^*) = \sum_{j \in \mathcal{J} \cup \mathcal{B}} (\mathcal{R}(u^*)_j)^{q-1} \nabla [\mathcal{R}(u^*)_j] = \sum_{j \in \mathcal{J} \cup \mathcal{B}} w_j \nabla [\mathcal{R}(u^*)_j].$$

Note that $\nabla [\mathcal{R}(u^*)_j]$ is the j -th row of the Jacobian matrix $D\mathcal{R}(u^*)$, which is given by (11)–(12) if $j \in \mathcal{J}$, and by (13) if $j \in \mathcal{B}$. Hence, we can write $\nabla L(u^*) = 0$ as

$$(D\mathcal{R}(u^*))^\top w = 0, \quad (14)$$

where $(D\mathcal{R}(u^*))^\top$ denotes the matrix transpose of $D\mathcal{R}(u^*)$. Since $D\mathcal{R}(u^*)$ is invertible, so is its transpose, and then we deduce that $w = 0$, implying that $\mathcal{R}(u^*) = 0$.

For the general case, since $0 \in \partial L(u^*)$ in \mathbb{R}^{M+N} , by Caratheodory's Theorem, there exist $K = M+N+1$ sequences $(u_n^{(k)})_n \subset \mathbb{R}^{M+N}$, with $k = 1, \dots, K$, and positive constants $\alpha_k > 0$ with $\sum_{k=1}^K \alpha_k = 1$ such that $L(u)$ is differentiable at $u_n^{(k)}$ for every n and k , $u_n^{(k)} \rightarrow u^*$ as $n \rightarrow \infty$ for all k , and

$$\sum_{k=1}^K \alpha_k \lim_{n \rightarrow \infty} \nabla L(u_n^{(k)}) = \lim_{n \rightarrow \infty} \sum_{k=1}^K \alpha_k (D\mathcal{R}(u_n^{(k)}))^\top w_n^{(k)} = 0,$$

where $w_n^{(k)} = [\mathcal{R}(u_n^{(k)})]^{p-1}$ is the residual function associated to every term in the sequences.

Due to the continuity of the residual function $\mathcal{R}(u)$, we have $w_n^{(k)} \rightarrow w$ as $n \rightarrow \infty$ for all k , where $w = [\mathcal{R}(u^*)]^{p-1}$. We know from Lemma 1, that the matrix $(D\mathcal{R}(u_n^{(k)}))^\top$ is μ -diagonally dominant with μ independent of n and k . Moreover, since these operators are finite-dimensional matrices with uniformly bounded coefficients, by a compactness argument, we deduce the existence of matrices A_1, \dots, A_K such that, through a subsequence, we have

$$\lim_{n \rightarrow \infty} (D\mathcal{R}(u_n^{(k)}))^\top = A_k, \quad \text{for } k = 1, \dots, K.$$

Hence,

$$0 = \lim_{n \rightarrow \infty} \sum_{k=1}^K \alpha_k \left(D\mathcal{R}(u_n^{(k)}) \right)^\top w_n^{(k)} = \sum_{k=1}^K \alpha_k A_k w.$$

By the same argument as in step 1, the matrix $\sum_{k=1}^K \alpha_k A_k$ is also μ -diagonally dominant, and we conclude that $w = 0$, implying that $\mathcal{R}(u^*) = 0$. \square

2.2 Stability

We denote $\|u\|_{\ell^\infty(\mathcal{J})} \equiv \|(u_j)_{j \in \mathcal{J}}\|_\infty := \max_{j \in \mathcal{J}} |u_j|$. and $\|b\|_{\ell^\infty(\mathcal{B})} := \max_{j \in \mathcal{B}} |b_j|$ (or simply $\|u\|_\infty$ or $\|b\|_\infty$ when there is no ambiguity).

We recall the following stability result.

Theorem 2 (Stability). *Let assumptions (H0) – (H3) hold. Let u and $\mathcal{R}(u)$ be such that:*

$$\begin{aligned} \mathcal{H}(x_j, u_j, \nabla_G u_j) &= \mathcal{R}(u)_j, & j \in \mathcal{J} \\ u_j &= \bar{b}_j, & j \in \mathcal{B} \end{aligned}$$

and let v be such that

$$\begin{aligned} \mathcal{H}(x_j, v_j, \nabla_G v_j) &= 0, & j \in \mathcal{J} \\ v_j &= \bar{c}_j, & j \in \mathcal{B}. \end{aligned}$$

Then it holds

$$\|u - v\|_\infty \leq \max \left(\|\bar{b} - \bar{c}\|_{\ell^\infty(\mathcal{B})}, \frac{1}{\lambda} \|\mathcal{R}(u)\|_\infty \right). \quad (15)$$

Proof. We will use some (rather standard) comparison principle idea in the discrete case. Let us prove that

$$M := \max_{j \in \mathcal{J} \cup \mathcal{B}} (u_j - v_j)_+ \leq \max \left(\max_{j \in \mathcal{B}} (g_j - \bar{c}_j)_+, \frac{1}{\lambda} \|\mathcal{R}(u)_+\|_\infty \right),$$

where $x_+ := \max(x, 0)$ and $\mathcal{R}(u)_+ = ((\mathcal{R}(u)_j)_+)_j \in \mathcal{J}$. Let $M_B := \max_{j \in \mathcal{B}} (g_j - \bar{c}_j)_+$. Assume on the contrary $M > \max(M_B, \frac{1}{\lambda} \|\mathcal{R}(u)_+\|_\infty)$. In that case, $M > M_B \geq \max_{j \in \mathcal{B}} g_j - \bar{c}_j$. Then the maximum M is reached in the interior set \mathcal{J} : $\exists j \in \mathcal{J}$, $M = u_j - v_j$. In particular, $\forall k \in \mathcal{V}_j$, $u_j - v_j \geq u_k - v_k$, from which we obtain $\nabla_G u_j \geq \nabla_G v_j$.

Using (H2) and (H3), we deduce that

$$\begin{aligned} \mathcal{R}(u)_j &= \mathcal{H}(x_j, u_j, \nabla_G u_j) - \mathcal{H}(x_j, v_j, \nabla_G v_j) \\ &\geq \mathcal{H}(x_j, u_j, \nabla_G v_j) - \mathcal{H}(x_j, v_j, \nabla_G v_j) \geq \lambda(u_j - v_j). \end{aligned}$$

Hence $M = u_j - v_j \leq \frac{1}{\lambda} \mathcal{R}(u)_j \leq \frac{1}{\lambda} \|\mathcal{R}(u)_+\|_\infty < M$, which is a contradiction.

We can prove in the same way that

$$\min_{j \in \mathcal{J} \cup \mathcal{B}} (u_j - v_j)_- \geq \min \left(\min_{j \in \mathcal{B}} (g_j - \bar{c}_j)_-, \frac{1}{\lambda} \|\mathcal{R}(u)_-\|_\infty \right).$$

Combining the previous bounds, we obtain the desired result. \square

Next, we compare the function u , which satisfies

$$\mathcal{H}(x, u(x), \nabla_G u(x)) = \mathcal{R}(u)(x), \quad x \in \Omega \quad (16)$$

and approximate boundary conditions

$$u(x) = b(x), \quad x \in \partial\Omega \quad (17)$$

(for some bounded function b) together with the exact scheme solution $(v_j)_{j \in \mathcal{J}}$.

Proposition 1. *Assume Ω is a bounded domain with piecewise regular boundary $\partial\Omega$, and that $g_j = \bar{b}(x_j)$ on the boundary, for some bounded function \bar{b} , $\{x_j, j \in \mathcal{J}\} \subset \Omega$ and $\{x_j, j \in \mathcal{B}\} \subset \partial\Omega$. The following error estimate holds:*

$$\|u - v\|_{\ell^\infty(\mathcal{J})} \leq \max\left(\frac{1}{\lambda} \|\mathcal{R}(u)\|_{L^\infty(\Omega)}, \|b - \bar{b}\|_{L^\infty(\partial\Omega)}\right). \quad (18)$$

Proof. We first have the bound $\max(\frac{1}{\lambda} \|\mathcal{R}(u)\|_{\ell^\infty(\mathcal{J})}, \|b(x_j) - g_j\|_{\ell^\infty(\mathcal{B})})$. Then we use the trivial bounds $\|\mathcal{R}(u)\|_{\ell^\infty(\mathcal{J})} \leq \mathcal{R}(u)\|_{L^\infty(\Omega)}$ and $\|b(x_j) - g_j\|_{\ell^\infty(\mathcal{B})} \leq \|b - \bar{b}\|_{L^\infty(\partial\Omega)}$. \square

We can interpret this as an *a posteriori* error estimate, since the right-hand side can be evaluated numerically (for instance, via stochastic sampling in space), providing a computable bound on the true scheme error between the computed values and the exact scheme solution.

2.3 Some examples of monotone numerical Hamiltonians

Two primary classes of monotone Hamiltonians are the **Lax-Friedrichs** scheme (based on artificial viscosity) and **Upwind** schemes (based on the direction of characteristic flow).

The Lax-Friedrichs Hamiltonian

The Lax-Friedrichs Hamiltonian includes a “viscosity” term proportional to the Graph Laplacian. This ensures that the scheme is monotone by explicitly coupling node i to all its neighbors in \mathcal{V}_i .

$$\mathcal{H}_{LxF}(x_i, u_i, \{u_j\}_{j \in \mathcal{V}_i}) := H(x_i, u_i, \nabla_G u_i) - \alpha_i \sum_{j \in \mathcal{V}_i} w_{ij}(u_j - u_i), \quad (19)$$

where $\nabla_G u_i$ is a centered gradient approximation (e.g., $\sum_j w_{ij} \frac{u_j - u_i}{2}$) and α_i is the viscosity coefficient satisfying $\alpha_i \geq \max_p |\partial_p H|$.

Upwind Schemes

Upwind schemes (often related to Godunov schemes) attempt to respect the direction of information flow (characteristics) by only using neighbors that are “upwind” of the current node i . These schemes typically have less numerical dissipation than Lax-Friedrichs but can be more complex to formulate for general non-convex Hamiltonians.

For the standard Eikonal equation $|\nabla u| = f(x)$, a common upwind discretization on graphs relies on the neighbor with the minimal value relative to distance:

$$\left(\max_{j \in \mathcal{V}_i} \frac{(u_i - u_j)_+}{\Delta_{ij}} \right) = f(x_i) \quad (20)$$

The notation $(z)_+ = \max(z, 0)$ ensures that only neighbors with values *lower* than u_i contribute to the gradient calculation. This mimics the causality of the continuous solution, where information flows from lower values (sources) to higher values. This scheme is first derived by Rouy and Tourin [13] for Cartesian grids.

More generally, there is the general formula of Godunov numerical Hamiltonians \mathcal{H}_G derived by Bardi and Osher [1] for any strictly convex Hamiltonian H . For example, in \mathbb{R}^2 ,

$$H_G(p_-, p_+; q_-, q_+) = \text{ext}_{p \in I[p_-, p_+]} \text{ext}_{q \in I[q_-, q_+]} H(p, q), \quad (21)$$

where $\text{ext}_{p \in I[a, b]} = \min_{p \in [a, b]}$ if $a \leq b$, and $\text{ext}_{p \in I[a, b]} = \max_{p \in [b, a]}$ if $a > b$. $I[a, b]$ denotes the closed interval bounded by a and b , and p_\pm, q_\pm denote the standard forward and backward differencing of u for u_x and u_y .

In [16], an explicit Godunov Hamiltonian from the general formula (21) is derived for the anisotropic Eikonal equation:

$$H(\nabla u) = \sqrt{au_x^2 + bu_y^2 - 2cu_xu_y} = r(x). \quad (22)$$

Kao et al. [9] extend the approach to general convex, homogeneous Hamiltonians $H(\nabla u) = R(x)$ by utilizing the Legendre transform (Bellman's formula).

2.4 Remarks on the strong monotonicity

Our results apply to systems with numerical Hamiltonians that satisfy the strong monotonicity conditions **(H3)**. For many Hamiltonians of practical interests, such as $H(x, \nabla u)$ including the eikonal term $|\nabla u|$, defining a corresponding consistent and monotone numerical Hamiltonian can be achieved in many ways.

One common approach is to use the Lax-Friedrichs numerical Hamiltonian with a sufficiently large constant, which introduces numerical diffusion.

It is also possible to artificially introduce a perturbative term, such as λu to the Hamiltonian. In certain cases, the solution of the perturbed equation can be related to the perturbed one through the so-called Kruzhkov transform. Let us consider a Hamiltonian of the form

$$H(x, p) = G(x, p) - f(x), \quad (23)$$

where $f(x) > 0$ and $G(x, p)$ is positively homogeneous of degree 1 in p , i.e., $G(x, \alpha p) = \alpha G(x, p)$ for all $\alpha > 0$.

With the change of variable $v := (1 - \exp(-\lambda u(x)))/\lambda$, we see that v solves

$$H(x, \nabla v) + \lambda f(x)v = 0. \quad (24)$$

Similarly, we may apply this transform to the time dependent equation

$$u_t + H(x, \nabla u) = 0, \quad (25)$$

where $\mathcal{H}(x, p)$ is positively homogeneous of degree 1 in p .

For the Eikonal equations, we have

$$\|\nabla u\| = f(x) \iff \|\nabla v\| + \lambda f(x)v = f(x),$$

and

$$u_t + \|\nabla u\| = 0 \iff v_t + \lambda v + \|\nabla v\| = 0.$$

The Kruzhkov transform admits a natural interpretation in the context of optimal control. If $u(x)$ represents the value function of an optimal control problem with additive running cost $f(x)$ (e.g., $u(x) = \inf \int_0^\tau f(y(s))ds$), the transformed variable v can be viewed as the value function of a problem with exponential discounting.

As a consequence of the “discounting”, the Kruzhkov transform may introduce conditioning issues when recovering the original variable u_h . The inverse transformation is given by $u = -\lambda^{-1} \ln(1 - \lambda v)$.

Let v_h be the numerical approximation of v with error $\varepsilon_h = v_h - v$. A first-order expansion of the inverse transform reveals how this error propagates to the recovered solution u_h :

$$u_h - u \approx \frac{du}{dv}(v) \cdot \varepsilon_h = \frac{1}{1 - \lambda v} \cdot \varepsilon_h.$$

Recalling that $1 - \lambda v = e^{-\lambda u}$, the error relationship becomes:

$$|u_h - u| \approx e^{\lambda u} |v_h - v|. \quad (26)$$

This indicates that errors in the numerical solution v_h are **exponentially magnified** by the value of the solution itself. For grid points where $u(x)$ is small (near the boundary or target set), the amplification factor $e^{\lambda u} \approx 1$, and the accuracy is preserved. However, for points “far” from the boundary where the cost $u(x)$ is large, the transformation compresses a large range of u values into a very small interval of v (crowding near the asymptote $1/\lambda$). Consequently, small truncation or round-off errors in v_h translate into massive errors in u_h .

3 Time dependent problems

While the time-dependent evolution equation

$$u_t(t, x) + F(x, u, \nabla_G u) = 0, \quad (t, x) \in \mathbb{R}^+ \times \mathbb{R}^d, \quad (27)$$

can formally be viewed as a special case of the general stationary framework (6) by defining an augmented variable $y = (t, x)$ and a Hamiltonian $\mathcal{H}(y, u, p_y) = p_t + F(x, u, p_x)$, this perspective somehow obscures fundamental structural differences that distinguish time from spatial dimensions.

The primary distinction lies in the **vanishing viscosity mechanism** used to select the unique physical (entropy) solution. In the generic stationary setting analyzed previously, the vanishing viscosity method involves a full elliptic perturbation:

$$-\epsilon \Delta_y u + H(y, u, \nabla_y u) = 0 \quad (\epsilon > 0).$$

Applying this blindly to the time-dependent setup would imply the presence of a second-order time derivative $-\epsilon u_{tt}$, rendering the equation elliptic in space-time. However, in physical models and standard numerical schemes, the regularization is inherently **parabolic**, affecting only the spatial variables:

$$u_t + F(x, u, \nabla_x u) = \epsilon \Delta_x u, \quad \epsilon > 0. \quad (28)$$

There is typically no second-order vanishing viscosity term in the time dimension (u_{tt}). This absence of temporal diffusion enforces strict **causality**: the solution at time t depends only on the history $[0, t]$, not on future times. Furthermore, the sign of the viscosity parameter ϵ is critical. Having $\epsilon > 0$ is essential for the well-posedness of the parabolic perturbation; a negative sign would lead to an ill-posed backward heat equation, violating the entropy conditions required to select the physically relevant weak solution. Consequently, while the algebraic structure of the Hamiltonian is linear in p_t , the analytical and numerical treatment of the time variable requires a distinction from the spatial variables to respect this causal, parabolic structure.

The setup

We define the fully discrete problem on the space-time product space $G \times \mathbb{T}$, where $G = (V, E, W)$ is the spatial **geometrical graph** specified in Section 2 and $\mathbb{T} = \{t_n\}_{0 \leq n \leq N}$ is the discrete time set. The time interval $[0, T]$ is discretized uniformly as $t_n = n\Delta t$ for $n \in \{0, 1, \dots, N\}$, with time step $\Delta t = T/N$. The problem unknowns are the values $u_j^n \approx u(x_j, t_n)$ located at the spatial vertices specified by V and every time-step t_n .

We consider implicit-in-time numerical discretizations of the form

$$\frac{u_j^n - u_j^{n-1}}{\Delta t} + \mathcal{F}(x_j, u_j^n, \nabla_G u_j^n) = 0, \quad \text{for } (j, n) \in \mathcal{J} \times \{1, 2, \dots, N\}. \quad (29)$$

We would like to solve this system of equations, coupled with the initial-boundary data

$$u_j^0 = g_j^0 \quad \text{for } j \in \mathcal{J} \quad \text{and} \quad u_j^n = b_j^n \quad \text{for } (j, n) \in \mathcal{B} \times \{1, 2, \dots, N\}. \quad (30)$$

In the context of the general setup discussed in the section 2, formula (29) appears to be

$$\mathcal{H}\left(t^n, x_j, u_j^n, \frac{u_j^n - u_j^{n-1}}{\Delta t}, \nabla_G u_j^n\right) = 0, \quad (31)$$

where the interior and boundary points of the space-time computational graph \tilde{G} are given by

$$\tilde{\mathcal{J}} := \mathcal{J} \times \{1, 2, \dots, N\} \quad \text{and} \quad \tilde{\mathcal{B}} := (\mathcal{J} \times \{0\}) \cup (\mathcal{B} \times \{1, 2, \dots, N\}),$$

respectively; and for any interior point $(n, j) \in \tilde{\mathcal{J}}$, the set of neighbors is given by

$$\tilde{V}_{(j,n)} := \{(i, n) : i \in \mathcal{V}_j\} \cup \{(j, n-1)\}.$$

We see that the results of section 2 apply to this case under conditions **(H1)**–**(H3)** on \mathcal{H} defined in (31). However, due to the linear dependence of \mathcal{H} with respect to the time derivative, and the causality of the solution, which propagates only forward in time, the assumption **(H3)** about the strict monotonicity of the numerical Hamiltonian with respect to the variable u can be relaxed. In this section we assume

(F1) $\mathcal{F}(x_j, \dots)$ is Lipschitz continuous for all j

(F2) $\mathcal{F}(x, u, p)$ is monotone in the variables p (i.e. $\mathcal{F}(x_j, u, \uparrow)$ for all j, u)

(F3) There exists $\lambda \in (0, 1)$ such that for every $j \in \mathcal{J}$, it holds that

$$\Delta t \frac{\partial \mathcal{F}}{\partial u}(x_j, u, p) \geq -\lambda, \quad \text{for a.e. } (u, p) \in \mathbb{R} \times \mathbb{R}^{|\mathcal{V}_j|} \quad (32)$$

Note that these assumptions allow for numerical Hamiltonians \mathcal{F} which are not necessarily monotone in u , provided the time-step Δt is sufficiently small. Moreover, for functions \mathcal{F} which are non-decreasing in the u variable, there is no restriction in the time-step.

Well-posedness of the discrete problem

We start by proving that the initial-boundary value problem (29)–(30) has a unique solution for any initial condition $g \in \mathbb{R}^{|\mathcal{J}|}$ and boundary data $b \in \mathbb{R}^{|\mathcal{B}| \times N}$. In view of the finite-difference equation (29), the solution at time t_n only depends on the solution at time t_{n-1} . Hence, we can prove existence and uniqueness of solution by a recursive argument.

Let us fix the initial values $u_j^0 = g_j^0$ for all $j \in \mathcal{J}$. The solution at time t_1 , given by the values $(u_j^1)_{j \in \mathcal{J}}$, satisfy the boundary value problem

$$\begin{cases} \frac{u_j^1 - g_j^0}{\Delta t} + \mathcal{F}(x_j, u_j^1, \nabla_G u_j^1) = 0, & \text{for } j \in \mathcal{J} \\ u_j^1 = b_j^1, & \text{for } j \in \mathcal{B}. \end{cases}$$

This falls in the setting of section 2 with

$$\mathcal{H}(x_j, u_j, \nabla_G u_j) = \frac{u_j - g_j}{\Delta t} + \mathcal{F}(x_j, u_j, \nabla_G u_j).$$

We see that this numerical Hamiltonian satisfies **(H1)** and **(H2)** due to **(F1)** and **(F2)**. Moreover, **(F3)** implies that

$$\frac{\partial}{\partial u} \mathcal{H}(x_j, u, p) = \frac{1}{\Delta t} + \frac{\partial}{\partial u} \mathcal{F}(x_j, u, p) > \frac{1 - \lambda}{\Delta t} > 0, \quad \text{for a.e. } (u, p) \in \mathbb{R} \times \mathbb{R}^{|\mathcal{V}_j|}, \quad (33)$$

so **(H3)** also holds. Therefore, by Theorem 1, values $(u_j^1)_{j \in \mathcal{J}}$ satisfying (29) exist and are unique. By a similar argument, if for any n , we assume that the values $(u_j^{n-1})_{j \in \mathcal{J}}$ satisfying (29) exist and are unique, we can prove that the values $(u_j^n)_{j \in \mathcal{J}}$ satisfying (29) also exist and are unique. Hence, by a recursive argument, we deduce existence and uniqueness of $(u_j^n)_{j \in \mathcal{J}}$ for every $n \geq 0$.

Uniqueness of critical points

Next, we prove that, for some $q > 1$ and $\mu_b, \mu_i > 0$, the unique solution of (29)–(30) is the unique critical point of a functional of the form

$$\begin{aligned} L(u) := & \frac{1}{qMN} \sum_{n=1}^N \sum_{j \in \mathcal{J}} \left[\frac{u_j^n - u_j^{n-1}}{\Delta t} + \mathcal{F}(x_j, u_j^n, \nabla_G u_j^n) \right]^q + \frac{\mu_b}{qM_b N} \sum_{n=1}^N \sum_{j \in \mathcal{B}} (u_j^n - b_j^n)^q \\ & + \frac{\mu_i}{qM} \sum_{j \in \mathcal{J}} (u_j^0 - g_j^0)^q, \end{aligned} \quad (34)$$

where $M = |\mathcal{J}|$ and $M_b = |\mathcal{B}|$. We can write $L(u) = \frac{1}{q} \|\mathcal{R}(u)\|_q^q$, where $\mathcal{R}(u)$ is the residual function

$$\mathcal{R}(u)_j^n := \begin{cases} \left(\frac{1}{MN}\right)^{1/q} \left(\frac{u_j^n - u_j^{n-1}}{\Delta t} + \mathcal{F}(x_j, u_j^n, \nabla_G u_j^n) \right) & (j, n) \in \mathcal{J} \times \{1, 2, \dots, N\}, \\ \left(\frac{\mu_b}{M_b N}\right)^{1/q} (u_j^n - b_j^n) & (j, n) \in \mathcal{B} \times \{1, 2, \dots, N\}, \\ \left(\frac{\mu_i}{M}\right)^{1/q} (u_j^0 - g_j^0) & (j, n) \in \mathcal{J} \times \{0\}. \end{cases} \quad (35)$$

We see that u is a solution of (29)–(30) if and only if $\mathcal{R}(u) = 0$.

Theorem 3 (Critical points - time dependent case). *Consider the loss function (34). We assume that \mathcal{F} satisfies **(F1)**, **(F2)**, **(F3)**. Then $L(u)$ has a unique critical point, in the sense that there is a unique u^* such that $0 \in \partial L(u^*)$, and this critical point is the unique solution of (29)–(30).*

Proof. We can write the functional $L(u)$ in (34) as

$$L(u) = \frac{1}{qN} \sum_{n=1}^N \|\mathcal{R}(u)^n\|_q^q + \frac{\mu_i}{pM} \sum_{j \in \mathcal{J}} (u_j^0 - g_j^0)^q \quad (36)$$

where, for each $1 \leq n \leq N$, $\mathcal{R}(u)^n \in \mathbb{R}^{|\mathcal{J} \cup \mathcal{B}|}$ is defined as

$$[\mathcal{R}(u)^n]_j := \begin{cases} \frac{1}{M^{1/q}} \left(\frac{u_j^n - u_j^{n-1}}{\Delta t} + \mathcal{F}(x_j, u_j^n, \nabla_G u_j^n) \right) & j \in \mathcal{J}, \\ \left(\frac{\mu_b}{M_b}\right)^{1/q} (u_j^n - b_j^n) & j \in \mathcal{B}. \end{cases} \quad (37)$$

Let $u = (u_j^n)_{j \in \mathcal{J} \cup \mathcal{B}}^{0 \leq n \leq N}$ be a critical point of L . We shall consider only the case when the functional L is differentiable at u . The generalization to the non-differentiable case can be done in a similar way as in Theorem 1. The proof is done by recurrence over n . We shall first prove that $\mathcal{R}(u)^N = 0$, and then, for any $n \in \{0, \dots, N-1\}$, we shall prove that $\mathcal{R}(u)^{n+1} = 0$ implies $\mathcal{R}(u)^n = 0$.

Step 1: Since u is a critical point of $L(u)$, we have that $\frac{\partial}{\partial u_j^N} L(u) = 0$ for all $j \in \mathcal{J} \cup \mathcal{B}$. In view of (36) and (37), we see that the terms u_j^N only appear in the term $\|\mathcal{R}(u)^N\|_p^p$ of the functional. Therefore, $\frac{\partial}{\partial u_j^N} L(u) = 0$ for all $j \in \mathcal{J} \cup \mathcal{B}$ implies that

$$\nabla_{u^N} L(u) = \nabla_{u^N} \left(\frac{1}{q} \|\mathcal{R}(u)^N\|_q^q \right) = 0.$$

Notice that $\frac{1}{q} \|\mathcal{R}(u)^N\|_q^q$ as a function of u^N falls in the setting of Theorem 1, with \mathcal{H} given by

$$\mathcal{H}(x_j, u_j^N, \nabla_G u_j^N) = \frac{u_j^N - u_j^{N-1}}{\Delta t} + \mathcal{F}(x_j, u_j^N, \nabla_G u_j^N).$$

We see that **(H3)** implies (33), and therefore, conditions **(F1)–(F3)** on \mathcal{F} imply that \mathcal{H} satisfies **(H1)–(H3)**. Hence, Theorem 1 ensures that $\mathcal{R}(u)^N = 0$.

Step 2: For any $1 \leq n \leq N-1$, let us now assume that $\mathcal{R}(u)^{n+1} = 0$. We see that the terms u_j^n with $j \in \mathcal{J} \cup \mathcal{B}$ only appear in the terms $\|\mathcal{R}(u)^n\|_q^q$ and $\|\mathcal{R}(u)^{n+1}\|_q^q$ of the functional $L(u)$, as defined in (36). Hence, $\frac{\partial}{\partial u_j^n} L(u) = 0$ for all $j \in \mathcal{J} \cup \mathcal{B}$ implies

$$\nabla_{u^n} \left(\frac{1}{q} \|\mathcal{R}(u)^n\|_q^q + \frac{1}{q} \|\mathcal{R}(u)^{n+1}\|_q^q \right) = 0,$$

and since we assumed that $\mathcal{R}(u)^{n+1} = 0$, we have $\nabla_{u^n} \left(\frac{1}{q} \|\mathcal{R}(u)^n\|_q^q \right) = 0$. By the same argument as in step 1, we can use Theorem 1 to deduce that $\mathcal{R}(u)^n = 0$.

Step 3: It only remains to prove that $u_j^0 = g_j^0$ for all $j \in \mathcal{J}$. We note that the term u_j^0 in $L(u)$ only appears in the term $(u_j^0 - g_j^0)^q$, and in $\mathcal{R}(u)_j^1$ with $j \in \mathcal{J}$. Hence,

$$\partial_{u_j^0} L(u) = \partial_{u_j^0} \left(\frac{1}{q} (\mathcal{R}(u)_j^1)^q + \frac{1}{q} (u_j^0 - g_j^0)^q \right).$$

Since we proved in step 2 that $\mathcal{R}(u)_j^1 = 0$ for all $j \in \mathcal{J}$, we deduce that $\partial_{u_j^0} L(u) = 0$ implies $u_j^0 = g_j^0$ for all $j \in \mathcal{J}$. □

Existence, uniqueness, and stability of numerical solutions

Corollary 1. *Assume (F1)–(F3), the scheme (29) is well-defined.*

Proof. $\mathcal{H}(x_j, u, p) := \frac{u - u_j^n}{\Delta t} + \mathcal{F}(x_j, u, p)$ satisfies the assumptions of the previous theorem, with $\frac{\partial \mathcal{H}}{\partial u}(x_j, u, p) = \frac{1}{\Delta t} + \frac{\partial \mathcal{F}}{\partial u}(x_j, u, p) \geq \lambda := \frac{1}{\Delta t} - \left\| \left(\frac{\partial \mathcal{F}}{\partial u} \right)_- \right\|_\infty > 0$. □

Notice that in the case when \mathcal{F} does not depend on u (or is an increasing function of u), such as for the time-dependent eikonal equation $v_t + c(x)\|\nabla v\| = 0$, then there is no time step restriction ((F3) is always satisfied).

Theorem 4 (Stability, time-dependent case). *Assume **(H0)** and **(F1)–(F3)**. Let u^n, v^n satisfy:*

$$\frac{u_j^n - u_j^{n-1}}{\Delta t} + \mathcal{F}(x_j, u_j^n, Du_j^n) =: \mathcal{R}(u)_j^n, \quad j \in \mathcal{J} \tag{38}$$

$$\frac{v_j^n - v_j^{n-1}}{\Delta t} + \mathcal{F}(x_j, v_j^n, Dv_j^n) = 0, \quad j \in \mathcal{J} \tag{39}$$

with boundary conditions $u_j^n = \bar{b}_j^n$ and $v_j^n = \bar{c}_j^n$, $\forall j \in \mathcal{B}$. Then the following estimate holds:

$$\|u^{n+1} - v^{n+1}\|_\infty \leq \|u^n - v^n\|_\infty + \max(\Delta t \|\mathcal{R}(u)^{n+1}\|_\infty, \|\bar{b} - \bar{c}\|_{\ell^\infty(\mathcal{B})}).$$

Proof. By using similar arguments as for the stability of the steady state case. \square

In particular, by an immediate recursion, we deduce

$$\begin{aligned}\|u^n - v^n\|_\infty &\leq \|u^0 - v^0\|_\infty + \sum_{1 \leq m \leq n} \max(\Delta t \|\mathcal{R}(u)^m\|_\infty, \|\bar{b}^m - \bar{c}^m\|_{\ell^\infty(\mathcal{B})}). \\ &\leq \|u^0 - v^0\|_\infty + \Delta t \sum_{1 \leq m \leq n} \|\mathcal{R}(u)^m\|_\infty + \sum_{1 \leq m \leq n} \|\bar{b}^m - \bar{c}^m\|_{\ell^\infty(\mathcal{B})}\end{aligned}$$

This is a bound of the error with respect to the consistency error of the scheme $\mathcal{R}(u)$ and the boundary errors.

Explicit schemes

To put our contribution in context, we briefly discuss explicit time-marching schemes of the form

$$\frac{u_j^{n+1} - u_j^n}{\Delta t} + \mathcal{F}(x_j, u_j^n, \nabla_G u_j^n) = 0, \quad \text{for } (j, n) \in \mathcal{J} \times \{0, 1, \dots, N-1\}. \quad (40)$$

One can quickly derive an explicit recurrence relation for the residual $w_j^n = |\mathcal{R}(u)_j^n|^{q-1}$ at a given critical point of the correspondingly defined loss functional:

$$\begin{aligned}w_j^n &= \left(1 - \Delta t \mathcal{F}_u(x_j, u_j^n, \nabla_G u_j^n) - \sum_{k \in \mathcal{V}_j} \frac{\Delta t}{\Delta x_{jk}} \mathcal{F}_{p_k}(x_k, u_j^n, \nabla_G u_j^n) \right) w_j^{n+1} \\ &\quad + \sum_{k \in \mathcal{V}_j} \frac{\Delta t}{\Delta x_{jk}} \mathcal{F}_{p_k}(x_k, u_k^n, \nabla_G u_k^n) w_k^{n+1},\end{aligned}$$

for $n = N-1, \dots, 0$, starting with $w_j^N = 0$. The well-posedness of the residual minimization problem for explicit schemes holds easily. In particular, there is no restriction on the size of Δt in this regard, while the stability of time marching requires Δt to satisfy a CFL condition.

In contrast, the well-posedness of the class of implicit schemes under consideration requires some mild condition on Δt , see **(F3)**, while having a superior stability property.

4 Numerical algorithms

Here, we present the algorithms for solving Hamilton-Jacobi equations using monotone numerical Hamiltonians and gradient descent-based algorithms. Our interest is in constructing deep neural networks that approximately solve the given problems involving Hamilton-Jacobi equations, and the design consideration is that the algorithm should be easy to port to run on GPUs.

Deep feed-forward networks are not defined on any mesh or grid. Nevertheless, our approach, stemming from [6], does “collocate” equations defined by monotone numerical Hamiltonians at randomly selected points, called collocation points. Each collocation point, p , is regarded as a grid node in a uniform Cartesian grid $p + \Delta x \mathbb{Z}^d$, which corresponds to

the graph G used in Section 2. Consequently, we view the continuous domain \mathbb{R}^d as the union of all such shifted Cartesian grids, allowing the stochastic optimization to minimize the scheme's residual across the entire family of admissible graphs.

The set of collocation points is refreshed during gradient descent steps, and the parameters in the numerical Hamiltonians, such as Δx , λ (the artificial damping term), and α (the numerical viscosity coefficient in the Lax-Friedrichs Hamiltonian), can be revised as well. Hence, the loss functional is regarded as a function depending on these parameters:

$$L(u) \equiv L(\theta, \Delta x, \lambda, \alpha).$$

In the Appendix, we present **Algorithm 1**, which describes a stochastic gradient descent scheme for minimizing the residual functional defined by a numerical Hamiltonian and a graph. In other words, **Algorithm 1** optimizes $L(\theta, \Delta x, \lambda, \alpha)$ with respect to θ , with all other parameters fixed.

Typically, we intend to construct a sufficiently accurate approximation of the viscosity solution for a given Hamilton-Jacobi equation. Therefore, it is important that the proposed algorithm is efficient and scales favorably as Δx decreases. However, as we see from Lemma 1, the condition number of $D\mathcal{R}$ increases as Δx decreases (equivalently, as M and N increase). The increasing complexity of the numerical scheme as the grid is refined is a typical feature of numerical methods for solving partial differential equations.

Algorithm 1 SGD for a finite-difference residual minimization

Require: $\{\eta_k\}_{k=0}^K \in (0, \infty)^K$, $N_0, N_b \in \mathbb{N}$, \mathcal{J}, \mathcal{B} .
Input: $\theta_0 \in \Theta$, $\mathcal{G} = (V, E, W)$, $\alpha, \lambda > 0$, $u(\cdot, \theta) : x \in \mathbb{R}^d \mapsto \mathbb{R}$
procedure SGDMINRES($u, \theta_0, \mathcal{G}, \lambda, \alpha$)
 $k \leftarrow 0$
 while $k < K$ **do**
 $\tilde{\mathcal{J}} \leftarrow N_0$ i.i.d. samples from \mathcal{J}
 $\tilde{\mathcal{B}} \leftarrow N_b$ i.i.d. samples from \mathcal{D}_B
 $\tilde{L}(\theta^k, \lambda, \alpha) = \frac{1}{qN_0} \sum_{j \in \tilde{\mathcal{J}}} [\mathcal{H}(x_j, u(x_j, \theta^k), \nabla_G u(x_j, \theta^k))]^q + \frac{\mu_b}{qN_b} \sum_{j \in \tilde{\mathcal{B}}} (u(x_j, \theta) - g_j)^q$
 $\theta^{k+1} := \theta^k - \eta_k \nabla_\theta \tilde{L}(\theta^k, \lambda, \alpha)$
 $k \leftarrow k + 1$
 end while
 return θ^K
end procedure

A multi-level training algorithm

We advocate adopting a "warm-up" strategy to accelerate the computation. This can mean optimizing a sequence of loss functionals

$$L^{(k)}(\theta) := L(\theta, \Delta x^{(k)}, \lambda^{(k)}, \alpha^{(k)}), \quad k = 0, 1, \dots \quad (41)$$

starting with ones defined with larger damping or artificial viscosity, and on "coarser" graphs or grids, and then continue training the NN with a more accurate discretizations of the PDE. Such a general strategy is summarized in **Algorithm 2**.

In classical setups involving meshes and grids, such kind of strategies require additional interpolation/prolongation to map a numerical solution on a coarser mesh to a finer one. In our experience, the use of sufficiently expressive neural networks eliminates the need for this procedure and can result in significant acceleration, especially in higher-dimensional cases beyond the reach of classical methods.

In this section, we focus primarily on solving Hamilton-Jacobi equations in Euclidean domains and use uniform Cartesian grids.

Algorithm 2 Multilevel stochastic residual-norm gradient descent

Require: $M \in \mathbb{N}$, $L > 0$, $\mathcal{G}^{(m)} = (V^{(m)}, E^{(m)}, W^{(m)})$, $\{(\lambda^{(m)}, \alpha^{(m)})\}_{m=0}^M \in (0, \infty)^{2M}$.

Ensure: $\lambda^{(m+1)} \leq \lambda^{(m)}$, $\alpha^{(m+1)} \leq \alpha^{(m)}$ and $\Delta x^{(m+1)} \leq \Delta x^{(m)}$ for all $1 \leq m \leq 2M$.

Initialize $\theta_0 \in \Theta$ such that $x \mapsto u(x; \theta_0)$ has Lipschitz constant L .

$m \leftarrow 0$

while $m < M$ **do**

$\theta_{m+1} := \text{SGDMinRes}(u, \theta_m, \mathcal{G}^{(m)}, \alpha_m, \delta_m)$ as defined in Algorithm 1

$m \leftarrow m + 1$

end while

return θ_M

The benefit of "warm starting"

We consider the minimization of $u \mapsto L(u, h)$ defined on a grid with spacing $h > 0$. Let u_h^* denote its (unique) minimizer and define the loss *gap*

$$E_k := L(u^k, h) - L(u_h^*, h).$$

We assume that $L(\cdot, h)$ is differentiable and satisfies

$$\|\nabla L(u, h) - \nabla L(v, h)\|_h \leq C_h \|u - v\|_h \quad \forall u, v, \quad (42)$$

$$L(u, h) - L(u_h^*, h) \geq \frac{\mu_h}{2} \|u - u_h^*\|_h^2 \quad \forall u. \quad (43)$$

In Lemma 1, we derived a lower bound for μ_h to be $O(h)$ so the condition number

$$\kappa_h := \frac{C_h}{\mu_h} = O(h^{-1}).$$

Thus, gradient descent with the step size $\eta = 1/C_h$ leads to

$$E_k \leq (1 - \kappa_h^{-1})^{2k} E_0.$$

Consequently, the number of iterations required to reach $E_k \leq \text{tol}$ satisfies

$$k(h; E_0) = \left\lceil \frac{\log(E_0/\text{tol})}{\log(1/q_h^2)} \right\rceil \approx \frac{\kappa_h}{2} \log\left(\frac{E_0}{\text{tol}}\right),$$

where we used $\log(1/q_h^2) \sim 2/\kappa_h$ for large κ_h .

Two-level warm start

Let u_{2h} be an approximate minimizer of $L(u, 2h)$, defined by a neural network. We define the warm start on the fine grid by the restriction of the neural network, u_{2h} , on the fine grid:

$$u_0^{\text{warm}} := u_{2h}.$$

Assume discretization consistency at the level of minimizers:

$$\|u_h^* - \mathcal{P}u_{2h}^*\|_h \leq Ch^p, \quad p > 0,$$

where \mathcal{P} represents the mapping of the neural network solution to the fine grid. Although our implementation evaluates the network directly without explicit matrix multiplication, for analysis purposes, we treat this evaluation as the operator \mathcal{P} .

Using only the Lipschitz continuity of the gradient, the initial fine-grid loss gap satisfies

$$E_{\text{warm}}(h) = L(u_0^{\text{warm}}, h) - L(u_h^*, h) \lesssim \frac{C_h}{2} \|u_{2h} - u_h^*\|_h^2.$$

If the coarse problem is solved to a comparable loss tolerance so that the mapped coarse optimization error is below the tolerance, then

$$E_{\text{warm}}(h) \lesssim \tilde{C}_h h^{2p} + \text{tol}.$$

Net iteration gain. Let E_{rand} denote the initial loss gap on the fine grid associated with a random initialization. The iteration count for a direct fine-grid solve is

$$k_{\text{direct}}(h) \approx \frac{\kappa_h}{2} \log\left(\frac{E_{\text{rand}}}{\text{tol}}\right).$$

The total iteration count for the two-level strategy is defined as

$$k_{2\text{lvl}}(h) := k_{\text{coarse}}(2h) + k_{\text{warm}}(h),$$

where

$$k_{\text{coarse}}(2h) \approx \frac{\kappa_{2h}}{2} \log\left(\frac{E_{\text{rand}}^{(2h)}}{\text{tol}}\right), \quad k_{\text{warm}}(h) \approx \frac{\kappa_h}{2} \log\left(\frac{E_{\text{warm}}(h)}{\text{tol}}\right).$$

Using $\kappa_{2h} \approx \kappa_h/2$, this yields the net reduction in iterations

$$\Delta k_{\text{net}}(h) := k_{\text{direct}}(h) - k_{2\text{lvl}}(h) \approx \frac{\kappa_h}{2} \log\left(\frac{E_{\text{rand}}}{E_{\text{warm}}(h)}\right) - \frac{\kappa_h}{4} \log\left(\frac{E_{\text{rand}}}{\text{tol}}\right).$$

This shows that “warm starting” does reduce the total number of needed iterations.

5 Numerical examples

In this section, we present numerical experiments designed to illustrate three distinct theoretical and practical advantages of the proposed framework: the spectral properties of the minimization problem, the capability to handle high-dimensional geometric constraints, and the robustness of the scheme for non-convex Hamiltonians.

First, in Section 5.1, we utilize a 1-dimensional Eikonal equation to empirically verify the condition number analysis derived in Lemma 1. This controlled setting allows us to isolate the impact of the discretization parameter Δx on the convergence rate of gradient descent. We demonstrate that the optimization landscape becomes increasingly stiff as the grid is refined, validating the necessity of the multi-level “warm-start” strategy (Algorithm 2) proposed in Section 4.

Second, in Section 5.2, we address the challenge of geometric complexity in high dimensions. We solve a time-dependent obstacle problem in \mathbb{R}^6 . While reference [6] established the method’s scalability for standard Eikonal equations, this example demonstrates that the framework successfully adapts Level Set Methods to high-dimensional settings with rigid constraints, a regime where the absence of a spatial mesh is a critical advantage.

Finally, in Section 5.3, we examine the case of non-convex Hamiltonians by solving a Hamilton-Jacobi-Isaacs equation arising in stochastic differential games [8]. Unlike standard Eikonal equations, this problem involves a min-max operator (the difference of norms), which challenges the selection of the correct viscosity solution. This example highlights the importance of the monotonicity conditions (H1)-(H3) in ensuring that the residual minimization converges to the physically relevant weak solution.

5.1 Impact of discretization on training efficiency

5.1.1 Deterministic gradient descent over grid functions

Here we show how the condition number of the residual’s Jacobian, denoted by $D\mathcal{R}(u)$, impacts the time until convergence when minimizing the least-squares loss $L(u) = \|\mathcal{R}(u)\|_2^2$ through gradient descent. Recall the definition of the residual function $\mathcal{R}(u)$ defined in (8), and the lower bound for the smallest eigenvalue of the Jacobian of $\mathcal{R}(u)$ given in Lemma 1. In our first experiment, we implement full gradient descent to the functional $L(u)$ over the space of grid functions \mathbb{R}^N , where N is the number of grid points. This produces a deterministic sequence in \mathbb{R}^N that approximates the L^2 -gradient flow associated to the residual $\mathcal{R}(u)$.

For simplicity, we consider the 1D Eikonal equation in the unit interval $(0, 1)$ with zero boundary condition, on a uniform grid $\{j\Delta x : j \in \{0, 1, \dots, N\}\}$, where $\Delta x = 1/N$. In the residual function $\mathcal{R}(u)$ in (8), we use the Lax-Friedrichs numerical Hamiltonian given by

$$\mathcal{H}\left(u_j, \frac{u_j - u_{j-1}}{\Delta x}, \frac{u_j - u_{j+1}}{\Delta x}\right) = \left| \frac{u_{j+1} - u_{j-1}}{2\Delta x} \right| - \alpha \frac{u_{j+1} + u_{j-1} - 2u_j}{2\Delta x} + \lambda u_j - 1, \quad (44)$$

for $j \in \{1, 2, \dots, N-1\}$ with $\lambda = \alpha = 1$, and null-boundary data $u_0 = u_N = 0$. Note that \mathcal{H} satisfies (H1)–(H3).

Assuming that the weighting factor μ_b for the boundary term in $\mathcal{R}(u)$ satisfies $\mu_b/2 \geq \Delta x$ (in our experiment we used $\mu_b = 10$), Lemma 1 shows that the smallest eigenvalue of $D\mathcal{R}(u)$ is bounded from below by $\sqrt{\Delta x}$. This lower bound indicates that fast convergence of gradient descent applied to $L(u) = \|\mathcal{R}(u)\|_2^2$ can be ensured by choosing a large value of Δx . In Figure 1 (left), we see the evolution of the loss function during gradient descent iterations (with step 10^{-3}) applied to the map

$$u \in \mathbb{R}^{N+1} \longmapsto L(u) := \|\mathcal{R}(u)\|_2^2,$$

with the initialization $u_0 = (0, \dots, 0) \in \mathbb{R}^{N+1}$. The iterations $u_{n+1} = u_n - 10^{-3} \nabla L(u_n)$ are stopped when the L^∞ -norm of the residual reaches a value smaller than 10^{-3} . We used different values of N , represented by different colors ($N = 20, 40, 80, 60$). These choices of N correspond to different values of Δx in the numerical Hamiltonian. We can see that the stopping criterion is reached faster for bigger values of Δx . On the contrary, for the two smallest values of Δx , the stopping criterion is not reached after 10^5 iterations. We can see in Figure 2 (left) that the grid function u corresponding to the latter cases does not give a good approximation of the sought solution. In Figure 1 (right) we show that by using a training schedule as described in Algorithm 2 in the Appendix, one can efficiently minimize the residual functional $L(u) = \|\mathcal{R}(u)\|_2^2$, even for small values of Δx . The main idea is that, by using a good initialization, one can avoid the flatter regions of the loss landscape, in which the lower bound given in Lemma 1 is tight. In this experiment, we used the following procedure: for each value of N , and with $\Delta x = 1/N$, we minimize $L(u)$ using gradient descent over $u \in \mathbb{R}^{N+1}$ until the stopping criterion is reached ($\|\mathcal{R}(u)\|_\infty < 10^{-3}$). Then, we reduce Δx by increasing N , and interpolate the function u in the finer grid by taking constant values of u between the grid points from the previous iteration. With this initialization, we apply again gradient descent to $L(u)$ until the stopping criterion is reached. The same idea can be implemented using Neural Networks, where the interpolation between different grids is given by the same Neural Network.

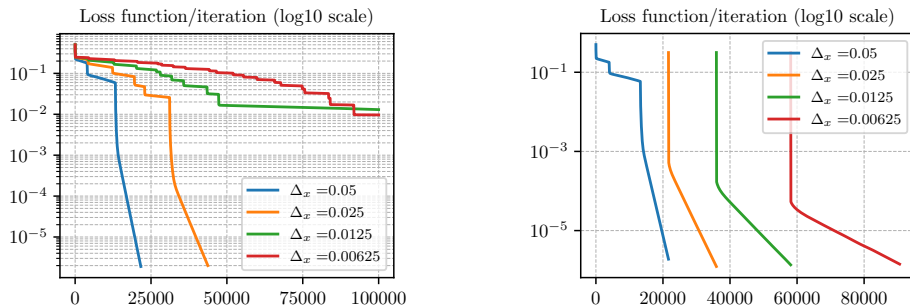


Figure 1: Evolution of the loss function $L(u) := \|\mathcal{R}(u)\|_2^2$ with different choices of Δx , from 0.05 to 0.00625. Full gradient descent is implemented in the space of grid functions \mathbb{R}^{N+1} , with $N = 1/\Delta x$. On the left, we see the evolution of the loss on a fixed grid, i.e. with constant Δx . On the right, we see the loss evolution on a varying grid with decreasing values of Δx . Every time the grid is refined, the grid function from the previous step is interpolated in the new grid by taking constant values between the former grid points.

In Figure 2 (center and right plots), we can see (in blue) the residual function $\mathcal{R}(u)$

associated to the last example shown in Figure 1 (left), i.e. the red plot. After 10^5 iterations of gradient descent applied to the grid function $u \in \mathbb{R}^{N+1}$, the solution has not converged to the sought solution due to the fact that the residual's Jacobian $D\mathcal{R}(u)$ is badly conditioned. The orange plots represent the two eigenvectors of the Jacobian matrix $D\mathcal{R}(u)$ associated to the smallest eigenvalue (approximately 0.079). We observe that, as expected, the loss function is a linear combination of these eigenvectors. Moreover, we see that the support of these eigenvectors, the size of which is proportional to Δx , is concentrated around the points where the red plot in Figure 1 has the wrong convexity.

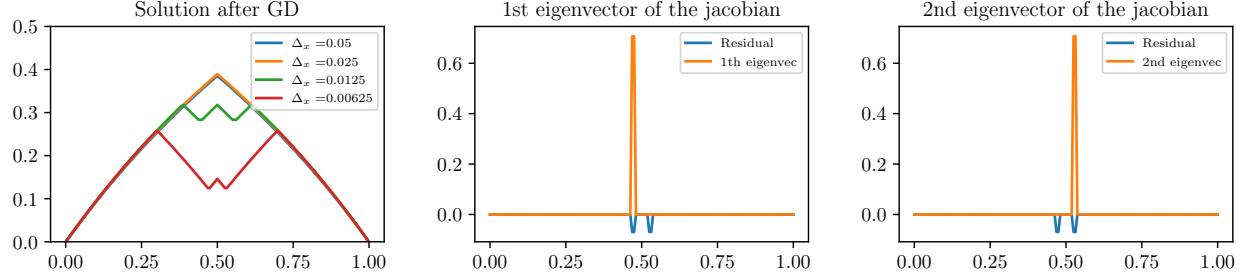


Figure 2: On the left, we see the solution u associated to the experiments in Figure 1 (left), for different values of Δx . On the center and right plots, for the last case (with $\Delta x = 0.00625$), we see (in blue) the residual function $\mathcal{R}(u)$ after 10^5 iterations of gradient descent; and (in orange) the eigenvectors of the Jacobian matrix $D\mathcal{R}(u)$ associated to the smallest eigenvalue (of size 0.079).

5.1.2 Implementation with Neural Networks and uniform sampling

In our next experiment, we verify that the same principle holds when the set of grid functions is replaced by a parametric family of continuous functions, that act as interpolator over the entire domain. We consider the same example as before, with the numerical Hamiltonian \mathcal{H} given by (44), with $\lambda = 0.1$ and $\alpha = 1$. In this case, the functional is given by

$$L(u) := \frac{1}{2} \int_0^1 [\mathcal{H}(u(x), D^+u(x), D^-u(x))]^2 dx + \frac{\mu_b}{2} (u(0)^2 + u(1)^2),$$

with $\mu_b = 10$. This choice ensures that the condition number of the residual's Jacobian is governed by $\sqrt{\Delta x}$. The parametric family of continuous functions that we use is a fully connected feedforward neural network with 3 hidden layers and 64 neurons per layer, that we denote by u_θ , with $\theta \in \mathbb{R}^p$ being the set of parameters. Here, $p = 12673$ is the number of parameters in the NN. We apply Adam optimization method with learning rate 10^{-3} to the function $\theta \mapsto L(u_\theta)$ for a maximum of 10^4 iterations. At each iteration, the integral term in $L(u)$ is approximated through Monte Carlo method, by taking 20 points (collocation points) uniformly at random in $(0, 1)$. As stopping criterion we use the condition of the average of the loss $L(u)$ over the last 50 iterations being smaller than 10^{-3} .

We compared the implementation of this method with different values of Δx , in particular $\Delta x = 1/20, 1/100$ and $1/1000$. Then, we implemented the same method using a training

schedule as proposed in Algorithm 2, with 4 training rounds. The values of λ at each round are 2, 1, 0.5 and 0.1, and the values of Δx are 1/20, 1/100, 1/500 and 1/1000. Since the initialization of the NN parameters and the collocation points in every iteration are different and randomly selected, we repeated each experiment 100 times independently. See Figure 3 for a summary of the experiments. The trained NN u_θ is viewed as an approximation of the PDE $|u'(x)| + \lambda u(x) = 1$ with $\lambda = 0.1$ and $u(0) = u(1) = 0$. Using the inverse Kruzhkov transform $v_\theta = \frac{1}{\lambda} \log \left(\frac{1}{1-\lambda u_\theta} \right)$, we have that v_θ is an approximation of the eikonal equation in $(0, 1)$ with null boundary conditions. The L^∞ -error in Figure 3 is computed as $\|v_\theta - v\|_\infty$, where v is the exact solution $v(x) = \min(x, 1-x)$.

As we can see in Figure 3, as we decrease Δx , the error after 10^4 iterations is worse in average. This happens because the NN can land in a flat region of the loss functional, where the loss decays very slowly. However, if we use a training schedule (training the NN with large values of λ and Δx first, and then decreasing them), we can ensure a small error, very consistently over the experiments.

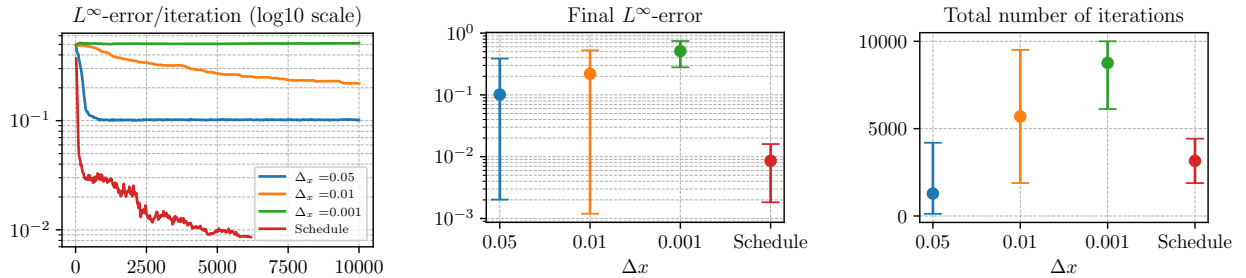


Figure 3: Summary of the experiments described in section 5.1.2, for the 1D eikonal equation. Each experiment was performed 100 times independently. In the last experiment (in red), we used a training schedule as in Algorithm 2, with Δx taking the values 1/20, 1/100, 1/500 and 1/1000 and λ taking the values 2, 1, 0.5 and 0.1. The left plot represents the evolution of the L^∞ -error in average over the 100 repetitions. The central plot represents the L^∞ -error at the end of the training procedure. On the right, we see the number of iterations before the stopping criterion was reached. In the two latter plots, points represent the mean over 100 i.i.d. experiments, and the intervals are delimited by the standard deviation.

5.2 Level set methods for the obstacle problem

To demonstrate the capability of our framework to handle high-dimensional geometry without spatial meshes, we solve a time-dependent non-linear advection problem in \mathbb{R}^5 with a rigid obstacle. The problem consists of finding the viscosity solution to

$$\begin{cases} \min \left(\frac{\partial u}{\partial t} + (a \cdot \nabla u)_+, \quad u(t, x) - \Psi(x) \right) = 0, & (t, x) \in (0, T] \times \Omega, \\ u(0, x) = g(x) := \max \left(\|x + a_0\|_2 - 1, \Psi(x) \right), & x \in \Omega, \end{cases} \quad (45)$$

on the domain $\Omega = [-2, 2]^6$, where $a_0 = (1, 1, \dots, 1) \in \mathbb{R}^6$, the direction of the drift is given by $a = \frac{a_0}{\|a_0\|}$, and the rigid obstacle is a ball of radius 1/2, centered at the origin, that we

represent by $\Psi(x)$ defined as

$$\Psi(x) = \|x\| - \frac{1}{2}. \quad (46)$$

Unlike classical Level Set Methods, which would require a grid of size N^6 (computationally prohibitive for any reasonable N), our method represents the solution by means of a parametrized Neural Network. In this example, we used a fully-connected multi-layer perceptron with 3 hidden layers and 80 neurons per layer, which in total contains 20081 parameters. The NN was trained using Adam optimizer, with learning rate $\eta = 0.001$, applied to the loss function

$$L(u) = \frac{1}{|\mathcal{X}|} \sum_{(t,x) \in \mathcal{X}} (\mathcal{R}(t,x))^2 + \frac{10}{|\mathcal{X}_0|} \sum_{x \in \mathcal{X}_0} (u(t,x) - g(x))^2,$$

where, for each iteration of Adam, \mathcal{X} is a batch of 10^4 points sampled uniformly at random in $(0, 2) \times (-2.5, 2.5)^5$, and \mathcal{X}_0 is a uniform sampling of $4 \cdot 10^3$ points in $(-2.5, 2.5)^5$. The residual function $\mathcal{R}(t, x)$ is based on an implicit discretization of the time-derivative, i.e.

$$\mathcal{R}(u(t,x)) = \min \left(\frac{u(t,x) - u(t - \Delta t, x)}{\Delta t} + \mathcal{H}(\nabla_{\Delta x} u(t,x)), u(t,x) - \Psi(x) \right).$$

As for the numerical Hamiltonian \mathcal{H} , we trained the NN for three rounds of 10^4 iterations each with a Lax-Friedrichs discretization of the form

$$\begin{aligned} \mathcal{H}(\nabla_{\Delta x} u(t,x)) := & \left(\sum_{i=1}^5 \frac{u(t, x + \Delta x e_i) - u(t, x - \Delta x e_i)}{2\Delta x} \right)_+ \\ & - \sum_{i=1}^5 \frac{u(t, x + \Delta x e_i) + u(t, x - \Delta x e_i) - 2u(t,x)}{2\Delta x}, \end{aligned}$$

with decreasing values of Δx and Δt . In particular, we used $\Delta x = \{0.3, 0.2, 0.1\}$ and $\Delta t = \{0.15, 0.1, 0.05\}$. Then, we switched to a higher-order scheme of the form

$$\mathcal{H}(\nabla_{\Delta x} u(t,x)) = \left(\sum_{i=1}^5 \frac{3u(t,x) - 4u(t,x - \Delta x e_i) + u(t,x - 2\Delta x e_i)}{2\Delta x} \right)_+.$$

With this numerical Hamiltonian, we trained again the NN for three rounds, applying 10^4 iterations of Adam in each rounds, again using decreasing values for the discretization steps. In particular, we used $\Delta x = \{0.2, 0.1, 0.05\}$ and $\Delta t = \{0.1, 0.05, 0.025\}$. Pre-training the NN with a Lax-Friedrichs Hamiltonian and large values of Δt ensures that the minimization problem is well-conditioned, which speeds up the training process. Note also that the use of an implicit discretization in time lifts the CFL condition on Δt . Then, in order to refine the result, we re-train the NN with a higher-order discretization and smaller Δt and Δx .

Figure 4 shows 2D cross-sections of the 5D solution, illustrating that the zero-level set successfully wraps around the obstacle constraints while maintaining the correct unit-speed propagation dynamics.

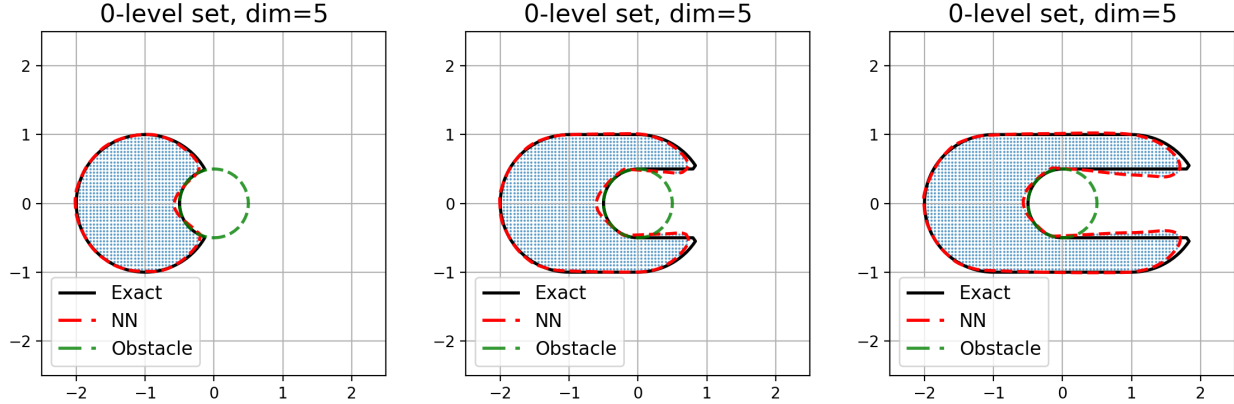


Figure 4: The zero-level set of the solution at time $t = 0$, $t = 1$ and $t = 2$. The figure represents a central 2D slice of the 5D domain, rotated so that the drift direction $a_0 = (1, 1, \dots, 1)$ corresponds to the positive direction of the x -axis.

5.3 A Hamilton-Jacobi-Isaacs equation

We consider an example from [8], which models a stochastic Zermelo reachability problem. The problem is posed on an annulus domain:

$$\Omega := \{(x, y) \in \mathbb{R}^2 : R^2 > x^2 + y^2 > r^2\}.$$

The value $v = v(x, y)$ is a solution of the following PDE:

$$-\frac{\sigma_x^2}{2}u_{xx} - \frac{\sigma_y^2}{2}u_{yy} - v_c(x, y)u_x + v_s\|\nabla u\|_2 - \kappa\|\nabla u\|_1 = 1, \quad x \in \Omega, \quad (47)$$

with boundary conditions

$$v = 0 \text{ on } S(0, r)$$

and

$$v = 1 \text{ on } S(0, R)$$

(the cost is minimal at the internal boundary $S(0, r)$ that we aim to reach, and is set to an arbitrary constant 1 at the external boundary $S(0, R)$ that we prefer to avoid). Here v_c represents a wind field in the x direction

$$v_c(x, y) := 1 - a \sin\left(\pi\left(\frac{x^2 + y^2 - r^2}{R^2 - r^2}\right)\right)$$

(the speed is maximal at the external boundary of the annulus), and some randomness in the model leads to the diffusion terms in (47). The parameters used here are

$$r = 0.5, R = \sqrt{2}, \kappa = 0.1, v_s = 0.5, a = 0.2, \sigma_x = 0.5, \sigma_y = 0.2.$$

Here the PDE is not convex neither concave in the unknown v . (Notice that the well-posedness of the PDE at the continuous level needs also a higher-order treatment of the boundary conditions - see [8], which we do not consider here for simplicity of presentation.)

Results are given in Figure 5. The numerical Hamiltonian used here is based on the following monotone finite difference approximations :

$$\|\nabla v\|_2 \simeq \sqrt{(DV_x^-)_+^2 + (DV_x^+)_+^2 + (DV_y^-)_+^2 + (DV_y^+)_+^2}$$

where

$$DV_x^\pm(x, y) := \frac{1}{h_x}(v(x, y) - v(x \pm h_x, y)), \quad DV_y^\pm(x, y) := \frac{1}{h_y}(v(x, y) - v(x, y \pm h_y)),$$

and

$$-\|\nabla v\|_1 \simeq \min(DV_x^-, DV_x^+) + \min(DV_y^-, DV_y^+),$$

and the usual second order approximations

$$\begin{aligned} -v_{xx} &\simeq \frac{-v(x - h_x, y) + 2v(x, y) - v(x + h_x, y)}{h_x^2}, \\ -v_{yy} &\simeq \frac{-v(x, y - h_y) + 2v(x, y) - v(x, y + h_y)}{h_y^2} \end{aligned}$$

A reference solution has been first computed by a finite difference scheme on a cartesian grid of 200^2 by embedding the problem into $[-2, 2]^2$ (a second order consistent scheme, see Fig 5, bottom).

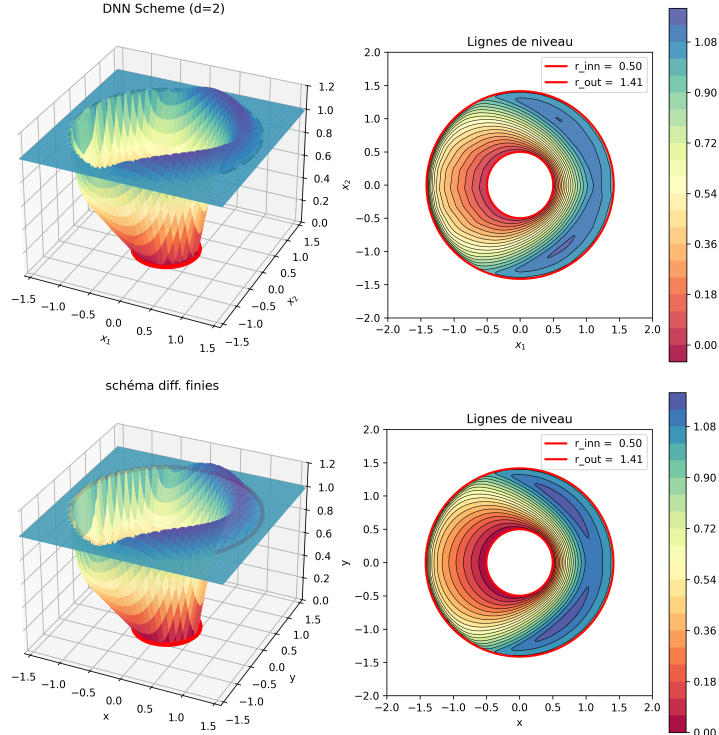


Figure 5: Above: DNN scheme, Below: reference solution

6 Conclusion

We have presented a framework for solving Hamilton-Jacobi equations by minimizing the L^q -norm of residuals arising from monotone finite-difference discretizations. By leveraging discrete monotonicity, our approach ensures convergence to the unique viscosity solution, directly addressing the non-uniqueness pitfalls of standard PINNs. We established the well-posedness of the minimization problem for a broad class of monotone discretizations and derived L^∞ error estimates that strictly bound the approximation error by the magnitude of the residual. Notably, for time-dependent problems, we showed that implicit time-stepping offers superior stability with only mild conditions for uniqueness. Furthermore, our spectral analysis confirms that the condition number scales inversely with grid spacing, suggesting the need for a multi-level “warm-start” strategy to accelerate training efficiency. Numerical results on high-dimensional obstacle problems and differential games demonstrate the method’s scalability and robustness. Future research will extend this analysis to higher-order accurate discretizations and degenerate parabolic equations on graphs.

Acknowledgments

Richard Tsai is supported partially by National Science Foundation grant DMS-2513857. Part of the research is also supported by the Swedish Research Council under grant no. 2021-06594, while the author was in residence at Institut Mittag-Leffler in Djursholm, Sweden during the Fall 2025 semester.

Esteve-Yagüe is supported by the Ministry of Science, Innovation and Universities of Spain under Ramón y Cajal grant RYC2022-035966-I.

References

- [1] M. Bardi and S. Osher. The nonconvex multidimensional riemann problem for hamilton–jacobi equations. *SIAM Journal on Mathematical Analysis*, 22(2):344–351, 1991.
- [2] G. Barles and P. E. Souganidis. Convergence of approximation schemes for fully non-linear second order equations. *Asymptotic analysis*, 4(3):271–283, 1991.
- [3] P. Chen, J. Darbon, and T. Meng. Lax-oleinik-type formulas and efficient algorithms for certain high-dimensional optimal control problems. *Communications on Applied Mathematics and Computation*, 6(2):1428–1471, 2024.
- [4] Y. T. Chow, J. Darbon, S. Osher, and W. Yin. Algorithm for overcoming the curse of dimensionality for state-dependent hamilton-jacobi equations. *Journal of Computational Physics*, 387:376–409, 2019.
- [5] J. Darbon and S. Osher. Algorithms for overcoming the curse of dimensionality for certain hamilton–jacobi equations arising in control theory and elsewhere. *Research in the Mathematical Sciences*, 3(1):19, 2016.

- [6] C. Esteve-Yagüe, R. Tsai, and A. Massucco. Finite-difference least square methods for solving hamilton-jacobi equations using neural networks. *Journal of Computational Physics*, 524:113721, 2025.
- [7] J. Hadamard. Sur les transformations ponctuelles. *Bull. Soc. Math. France*, 34:71–84, 1906.
- [8] K. Ito, C. Reisinger, and Y. Zhang. A neural network-based policy iteration algorithm with global H^2 -superlinear convergence for stochastic games on domains. *Found. Comput. Math.*, 21(2):331–374, 2021.
- [9] C.-Y. Kao, S. Osher, and Y.-H. Tsai. Fast sweeping methods for static hamilton–jacobi equations. *SIAM Journal on Numerical Analysis*, 42(6):2612–2632, 2005.
- [10] Y. Park and S. Osher. Neural implicit solution formula for efficiently solving hamilton–jacobi equations. *SIAM Journal on Scientific Computing*, 47(6):C1223–C1263, 2025.
- [11] B. H. Pourciau. Hadamard’s theorem for locally Lipschitzian maps. *J. Math. Anal. Appl.*, 85(1):279–285, 1982.
- [12] M. Raissi, P. Perdikaris, and G. E. Karniadakis. Physics-informed neural networks: A deep learning framework for solving forward and inverse problems involving nonlinear partial differential equations. *Journal of Computational physics*, 378:686–707, 2019.
- [13] E. Rouy and A. Tourin. A viscosity solutions approach to shape-from-shading. *SIAM Journal on Numerical Analysis*, 29(3):867–884, 1992.
- [14] J. A. Sethian. Fast marching methods. *SIAM review*, 41(2):199–235, 1999.
- [15] J. A. Sethian and A. Vladimirsky. Ordered upwind methods for static hamilton–jacobi equations. *Proceedings of the National Academy of Sciences*, 98(20):11069–11074, 2001.
- [16] Y.-H. R. Tsai, L.-T. Cheng, S. Osher, and H.-K. Zhao. Fast sweeping algorithms for a class of hamilton–jacobi equations. *SIAM Journal on Numerical Analysis*, 41(2):673–694, 2003.
- [17] J. N. Tsitsiklis. Efficient algorithms for globally optimal trajectories. *IEEE transactions on Automatic Control*, 40(9):1528–1538, 2002.
- [18] H. Zhao. A fast sweeping method for eikonal equations. *Mathematics of computation*, 74(250):603–627, 2005.